15 (2022) 100190

Contents lists available at ScienceDirect

International Journal of Thermofluids

journal homepage: www.sciencedirect.com/journal/international-journal-of-thermofluids

Numerical analysis of hybrid nanofluid natural convection in a wavy walled porous enclosure: Local thermal non-equilibrium model

Hakim T. Kadhim [a,*], Ahmed Al-Manea [a], Ali Najah Al-Shamani [a], Talal Yusaf [b]

[a] Mechanical Department, Al-Furat Al-Awsat Technical University, Kufa, Iraq
[b] School of Engineering and Technology, Central Queensland University, Australia

ARTICLE INFO

Keywords:
Natural convection
Hybrid nanofluid
Local thermal non-equilibrium
Wavy porous enclosure

ABSTRACT

A numerical study of the Buoyancy-driven flow in a porous enclosure, having a bottom heated wavy wall, filled with Cu-Al_2O_3/water hybrid nanofluid is performed using the local thermal non-equilibrium model. The non-dimensional governing equations of fluid flow and heat transfer are solved using the Galerkin finite element method. The state variables change in the porous enclosure is represented using the Darcy-Brinkman model. The impacts of various effective parameters which include nanoparticle volume fraction ($0 \leq \Phi \leq 0.04$), Darcy number ($10^{-5} \leq Da \leq 10^{-2}$), modified conductivity ratio ($0.1 \leq \gamma \leq 1000$), the number of undulations ($1 \leq N \leq 5$) and the amplitude of waviness ($0.05 \leq A \leq 2$).The results showed that the Darcy number is the first controlling parameter on the fluid flow and temperature distributions followed by *A, N* and γ. Additionally, the heat transfer rate is increased by increasing the thermal conductivity of the nanoparticles reaching its maximum value at $\Phi = 0.04$. Furthermore, by comparing the temperature fields of the fluid phase and solid matrix, it is clear that the effects of the local thermal non-equilibrium are significant at a low modified thermal conductivity ratio and high Darcy number.

1. Introduction

The study of natural convection inside a porous enclosure with wavy walls is crucial of importance, due to its use in many applications such as; electronic packages, microelectronic devices, heat exchangers, and solar heaters [1]. These enclosures can be filled with different working fluids. The use of hybrid nanofluid is a practical method for improving the thermal characteristics of heat transfer devices and reducing their size [2]. Kadhim, et al. [3] reported that adding copper–alumina nanoparticles in a wavy square enclosure shows a significant improvement in the rate of heat transfer compared to the pure fluid over a wide range of inclination angles. Chamkha, et al. [4] investigated the unsteady conjugate natural convective heat transfer inside a semi-circular enclosure filled with Al_2O_3Cu/water hybrid nanofluid. Among a wide range of the investigated effective parameters, it is reported that adding nanoparticles results in a significant enhancement in heat transfer at the solid-fluid interface. Alsabery, et al. [5] was also confirmed the enhancement in the heat transfer rate due to the use of hybrid nanofluid by studding the mixed convection inside a wavy lid-driven enclosure containing an adiabatic centred solid block. However, the natural convection studies of Mehryan, et al. [6] and Ghalambaz et al. [7] showed a reduction in the heat transfer performance by using hybrid nanofluid compared to the use of a nanofluid. Other numerical studies on enhancing heat transfer performance by using regular nanofluids or hybrid nanofluids can be found in the literature [8–13].

The use of a porous medium in an enclosure saturated with pure fluid or a fluid containing various nanoparticles or composite nanoparticles can enhance the heat transfer performance inside the enclosure. The increase in the permeability of the porous medium, which represents the Darcy number can reduce the convective flow resistance that generated due to the use of the porous medium. Kasaeian et al. [14] conducted a comprehensive review on the application of the CFD approach to predict the enhancement in the heat transfer performance of various enclosures using porous medium and nanofluids. Hashemi et al. [15] studied the free convection of Cu-water micropolar nanofluid in a porous enclosure with the existence of heat generation. The authors reported that increasing the Darcy number has a small impact on the micro-rotation of particles. Kadhim et al. [16] studied numerically free convective flow in a square composite layered cavity consisting of nanofluid and porous layers utilizing the finite difference method. A sinusoidal interface was utilized between the Cu-water nanofluid and the porous layer. The results showed that a high value of the Darcy number with lower porous layer thickness improve the heat transfer rate inside the cavity. More

* Corresponding author.
E-mail address: dw.hkm@atu.edu.iq (H.T. Kadhim).

https://doi.org/10.1016/j.ijft.2022.100190

Available online 5 August 2022

Nomenclature

Symbols

A	dimensionless amplitude
C_p	specific heat capacity (J kg^{-1} K^{-1})
Da	Darcy number
g	acceleration due to gravity (ms^{-2})
H	interphase heat transfer coefficient
k	thermal conductivity (W m^{-1}K^{-1})
K_r	thermal conductivity ratio
L	length and height of the enclosure (m)
N	wavy wall wavenumbers
Nu_{av}	average Nusselt number
Nu_s	local Nusselt number
p	pressure (Nm^{-2})
P	dimensionless pressure
Pr	Prandtl number
Ra	Rayleigh number
T	temperature (K)
u, v	components of velocity in the x and y directions (ms^{-1})
U, V	dimensionless components of velocity in the x and y directions
x, y	Cartesian coordinates (m)
X, Y	dimensionless Cartesian coordinates (m)

Greek symbols

α	thermal diffusivity (m^{2}s^{-1})
β	thermal expansion coefficient (K^{-1})
γ	modified conductivity ratio
ε	Porosity of the medium
θ	dimensionless temperature
μ	dynamic viscosity (kgm^{-1}s^{-1})
ν	kinematic viscosity (m^{2}s^{-1})
ρ	density (kgm^{-3})
ϕ	volume fraction of solids
ψ	stream function (m^{2}s^{-1})

Subscript

av	average
bf	pure fluid
c	cold
h	hot
hnf	hybrid nanofluid

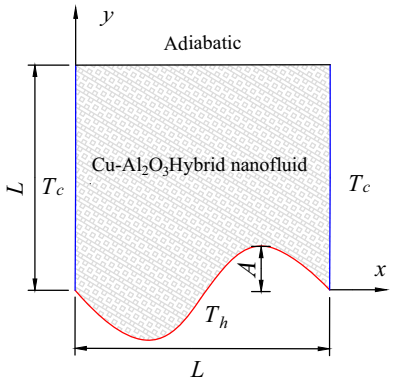

Fig. 1. The physical model of the hybrid nanofluid-porous enclosure.

Table 1
Mesh independence check at $N = 2$, $A = 0.1$, $Da = 10^{-3}$,$Ra = 10^6$,ϕ= 0.04.

Mesh size	Nu_{hnf}	Nu_s
70 × 70	15.227	13.147
90 × 90	15.282	13.197
110 × 110	15.312	13.225
130 × 130	15.377	13.287
150 × 150	15.387	13.289

interesting studies on natural convection heat transfer in an enclosure filled partially of fully with a porous medium can be found in [17–23].

The Thermal Equilibrium (LTE) model approach was mainly adopted in the majority of previous studies. Both the temperatures of the porous phase and fluid phase are considered to be equal in this approach. However, in a practical case, the Local Thermal Non-equilibrium (LTNE) model was reported as an accurate model to obtain the temperatures difference in many applications such as the cooling of electronic components and solar energy collectors [7]. Alsabery et al. [24] investigated by CFD free convection inside a square corrugated enclosure filled with Al_2O_3 water-based nanofluid with a vertical porous layer. It was found that the rate of heat transfer rate is increased by increasing the porosity for the solid and fluid phases. Izadi et al. [25] studied the convective heat transfer in a cavity filled with a porous media which is saturated by a nanofluid utilizing the Buongiorno LTNE model. The wavy sidewalls of the cavity are kept cold and a single pipe running through the enclosure is utilized for the heating. The findings showed the benefit of utilizing the LTNE model in which a great convective heat transfer is observed at the interface between the solid matrix and the working fluid.

In this study, a numerical investigation to study the effects of the Local Thermal Non-equilibrium (LTNE) and Cu-Al_2O_3-water hybrid nanofluid on the flow field and heat transfer in a porous wavy walled enclosure is presented. To the best of the authors' knowledge, there is no work reported on the natural convective flow within hybrid nanofluid under the effects of the LTNE model and a bottom-heated wavy wall. It aims to give an understanding to the impacts of Darcy number, amplitude, number of undulations, modified conductivity ratio for a varied range of nanoparticle volume fraction on flow, temperature distribution and the averaged Nusselt number using the Darcy-Brinkman model which is used widely to predict the flow in the porous media. The obtained results can contribute to essential performance enhancement and predicting fluid flow and heat transfer to various industrial applications.

2. Mathematical model

Fig. 1 shows a schematic diagram of the 2D wavy walled porous enclosure having the dimensions ($L \times L$) and filled with Cu-Al_2O_3/water hybrid nanofluid. A particular case is illustrated in Fig. 1, in which the amplitude of the bottom wavy wall is $A = 0.1$ and the number of undulations is $N = 2$. The bottom wavy wall is maintained with a uniform temperature while the horizontal top wall is assumed as an adiabatic wall. The right and left walls have uniform cold temperatures. In this study, the hybrid nanofluid is assumed laminar, incompressible, homogeneous mixture of water and Cu -Al_2O_3 nanoparticles. The physical properties of the Cu- Cu-Al_2O_3 /water hybrid nanofluid are illustrates in **Error! Reference source not found**. These properties are assumed with no variations, except for the density within the buoyancy term, which is determined utilizing the Boussinesq approximation. Cu-Al_2O_3 /water hybrid nanofluid is assumed to have a Newtonian behaviour, as indicated in [26].

In the current investigation, the porosity value (ε) of the porous medium is assumed to be a constant value of 0.5 with considering the

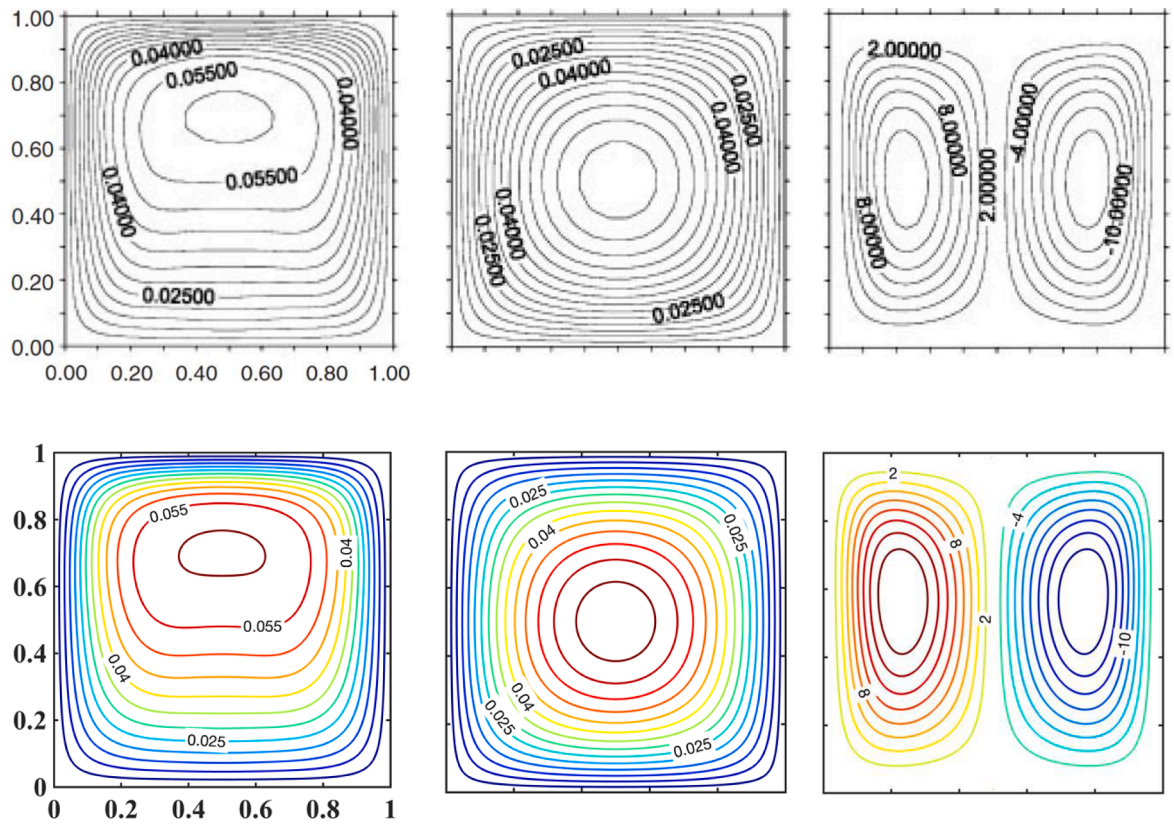

Fig. 2. Isotherms of the fluid phase (left) and solid phase(middle) and streamlines (right), Baytas [32], and current study (lower row), at $Da = 10^{-2}$, ε = 0.4, $Ra = 10^{7}$, $Pr = 7$,γ = 10^{-3}, $F_o = 5.648$ and $H = 500$.

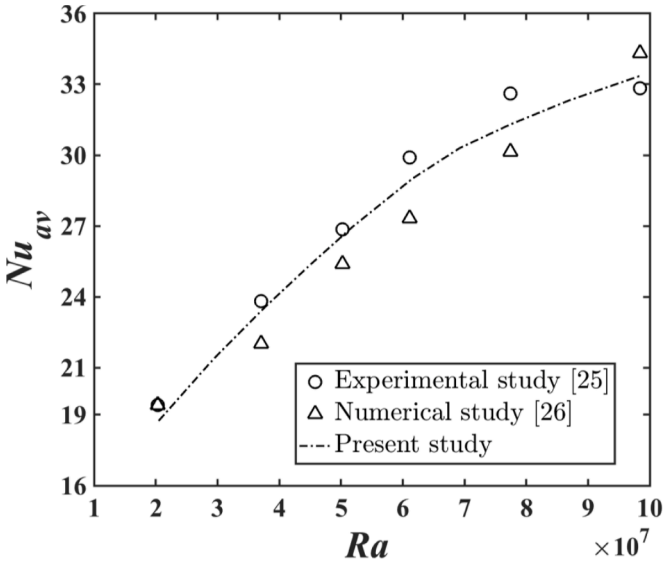

Fig. 3. Comparisons of the current numerical results with the experimental results of Putra, [33] and the numerical results of Corcione, [34] at various values of Rayleigh number.

effects of the permeability magnitude () in the Darcy number. Based on these assumptions, the equations of mass, momentum, and energy of the hybrid nanofluid including the nonequilibrium model are used as follows [27]

$$\frac{\partial U_{hnf}}{\partial X}+\frac{\partial V_{hnf}}{\partial Y}=0 \tag{5}$$

$$U_{hnf}\frac{\partial U_{hnf}}{\partial X}+V_{hnf}\frac{\partial U_{hnf}}{\partial Y}=-\frac{\partial P}{\partial X}+\frac{\rho_{bf}}{\rho_{hnf}\,(1-\varphi)^{2.5}}\times Pr\times\left(\frac{\partial^2 U_{hnf}}{\partial X^2}+\frac{\partial^2 U_{hnf}}{\partial Y^2}\right)-\frac{\rho_{bf}}{\rho_{hnf}\,(1-\varphi)^{2.5}}\times U_{hnf}\frac{Pr}{Da} \tag{6}$$

$$U_{hnf}\frac{\partial V_{hnf}}{\partial X}+V_{hnf}\frac{\partial V_{hnf}}{\partial Y}=-\frac{\partial P}{\partial Y}+\frac{\rho_{bf}}{\rho_{hnf}\,(1-\varphi)^{2.5}}\times Pr\times\left(\frac{\partial^2 V_{hnf}}{\partial X^2}+\frac{\partial^2 V_{hnf}}{\partial Y^2}\right)+\frac{(\rho\beta)_{hnf}}{\rho_{hnf}\beta_{bf}}\times Pr.Ra.\theta_{hnf}-\frac{\rho_{bf}}{\rho_{hnf}\,(1-\varphi)^{2.5}}\times V_{hnf}\frac{Pr}{Da} \tag{7}$$

$$U_{hnf}\frac{\partial \theta_{hnf}}{\partial X}+V_{hnf}\frac{\partial \theta_{hnf}}{\partial Y}=\frac{\alpha_{hnf}}{\alpha_{bf}}\left[\left(\frac{\partial^2\theta_{hnf}}{\partial X^2}+\frac{\partial^2\theta_{hnf}}{\partial Y^2}\right)+H\times\left(\theta_p-\theta_{hnf}\right)\right] \tag{8}$$

$$\frac{\partial^2\theta_p}{\partial X^2}+\frac{\partial^2\theta_p}{\partial Y^2}=\gamma\times H\times\left(\theta_{hnf}-\theta_p\right) \tag{9}$$

The non-dimensional variables below are used in Eqs. (5) to (9):

$$X=\frac{x}{L},\ Y=\frac{y}{L},\ U=\frac{uL}{\alpha_{bf}},\ V=\frac{vL}{\alpha_{bf}},\ P=\frac{pL^2}{\rho_{bf}\alpha_{bf}^2},\ Pr=\frac{\vartheta_{bf}}{\alpha_{bf}},\ \theta_{hnf}=\frac{T_{hnf}-T_c}{T_h-T_c},\ \theta_p=\frac{T_p-T_c}{T_h-T_c},$$

$$Ra=\frac{\beta.g.\Delta T.L^3}{\vartheta_{bf}.\alpha_{bf}},\ Da=\frac{K}{L^2},\ H=\frac{h\,L^2}{\varepsilon\,k_{hnf}},\ \gamma=\frac{\varepsilon\,k_{hnf}}{(1-\varepsilon)k_p}$$

The local and average Nusselt numbers along the bottom wavy wall is defined as in [28]:

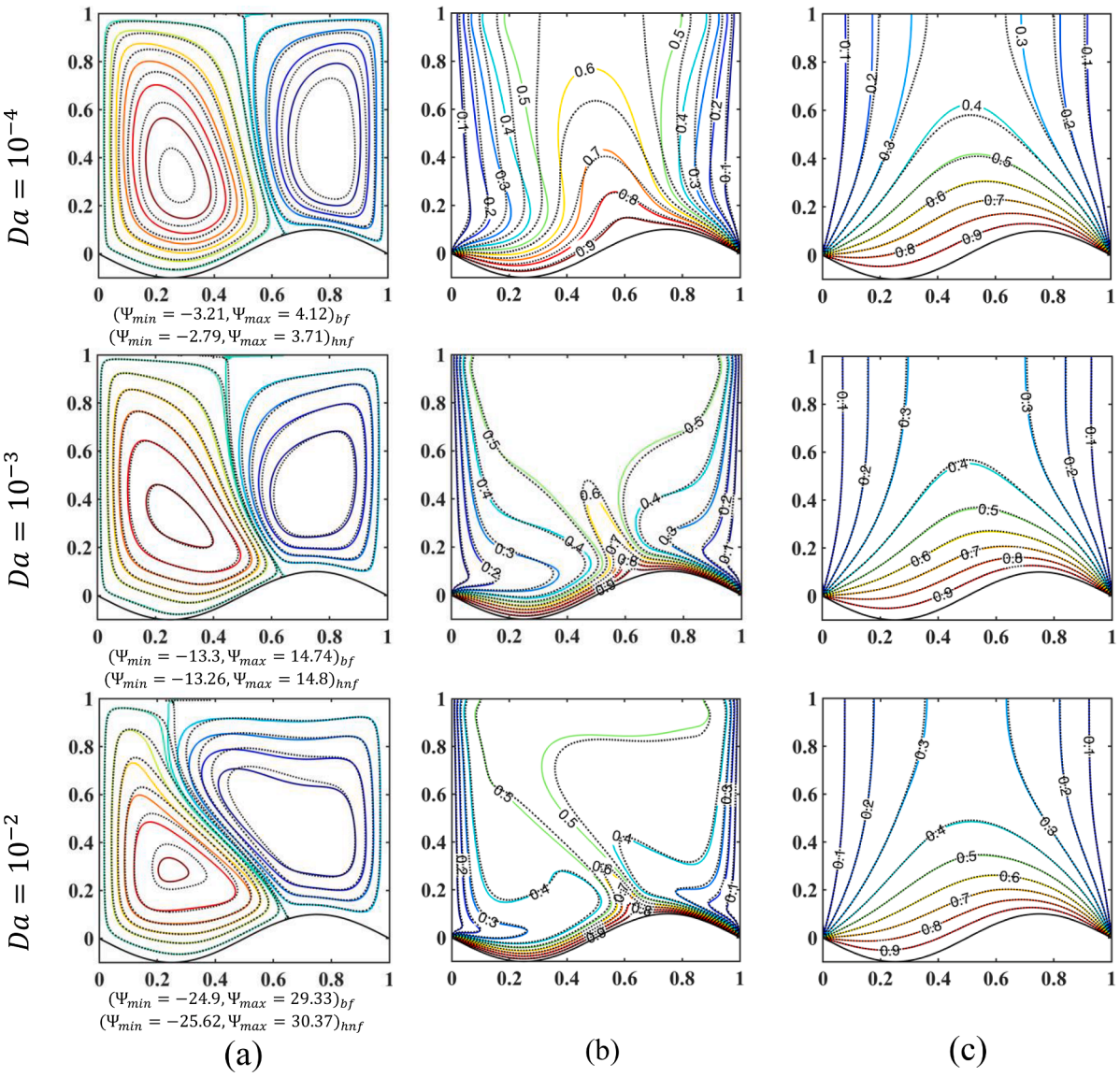

Fig. 4. Variations of (left column) streamlines, (middle column) isotherms of the hybrid nanofluid phase and (right column) isotherms of the solid phase for different Darcy numbers, at $\gamma = 10$,$A = 1$, $N = 2$, ϕ=0 (solid lines) and ϕ=0.04 (dashed lines).

$$Nu_{Local} = -\frac{k_{phase}}{k_{bf}}\frac{\partial\theta}{\partial n} \tag{10}$$

where k_{phase} represents k_s for the solid phase and k_{hnf} for the hybrid nanofluid phase and

$$Nu_{av} = \int_0^1 Nu_{Local}\, ds \tag{11}$$

where $\theta = \frac{T-T_c}{T_h-T_c}$ is the dimensionless temperature, n is the wavy wall inward normal direction, and s is the non-dimensional arc length of the wavy wall, where $0 \le s \le 1$ over $0 \le X \le 1$. Eq. (6)–(25)

The strength of the natural convective flow inside the enclosure is determined using the potential flow expression of [29] as follows:

$$\frac{\partial^2\Psi}{\partial X^2} + \frac{\partial^2\Psi}{\partial Y^2} = \frac{\partial U}{\partial Y} - \frac{\partial V}{\partial X} \tag{12}$$

The negative and positive signs of the streamfunction Ψ are indications for the flow directions.

The non-dimensional boundary conditions of the computational domain illustrated in Fig. 1, are:

- Along the bottom wavy wall of the cavity

  $U = V = 0,\ \theta_{hnf} = \theta_p = 1.$

- Along the right and left walls of the cavity

  $U = V = 0,\ \theta_{hnf} = \theta_p = 0.$

- Along the top wall of the enclosure

  $U = V = 0,\ \frac{\partial\theta_{hnf}}{\partial n} = 0.$

In the current study, the utilized thermophysical properties of hybrid nanofluid can be defined as follows [30,31]:

$$\rho_{hnf} = \varphi_{Al_2O_3}\rho_{Al_2O_3} + \varphi_{Cu}\,\rho_{Cu} + (1-\ \varphi)\rho_{bf} \tag{13}$$

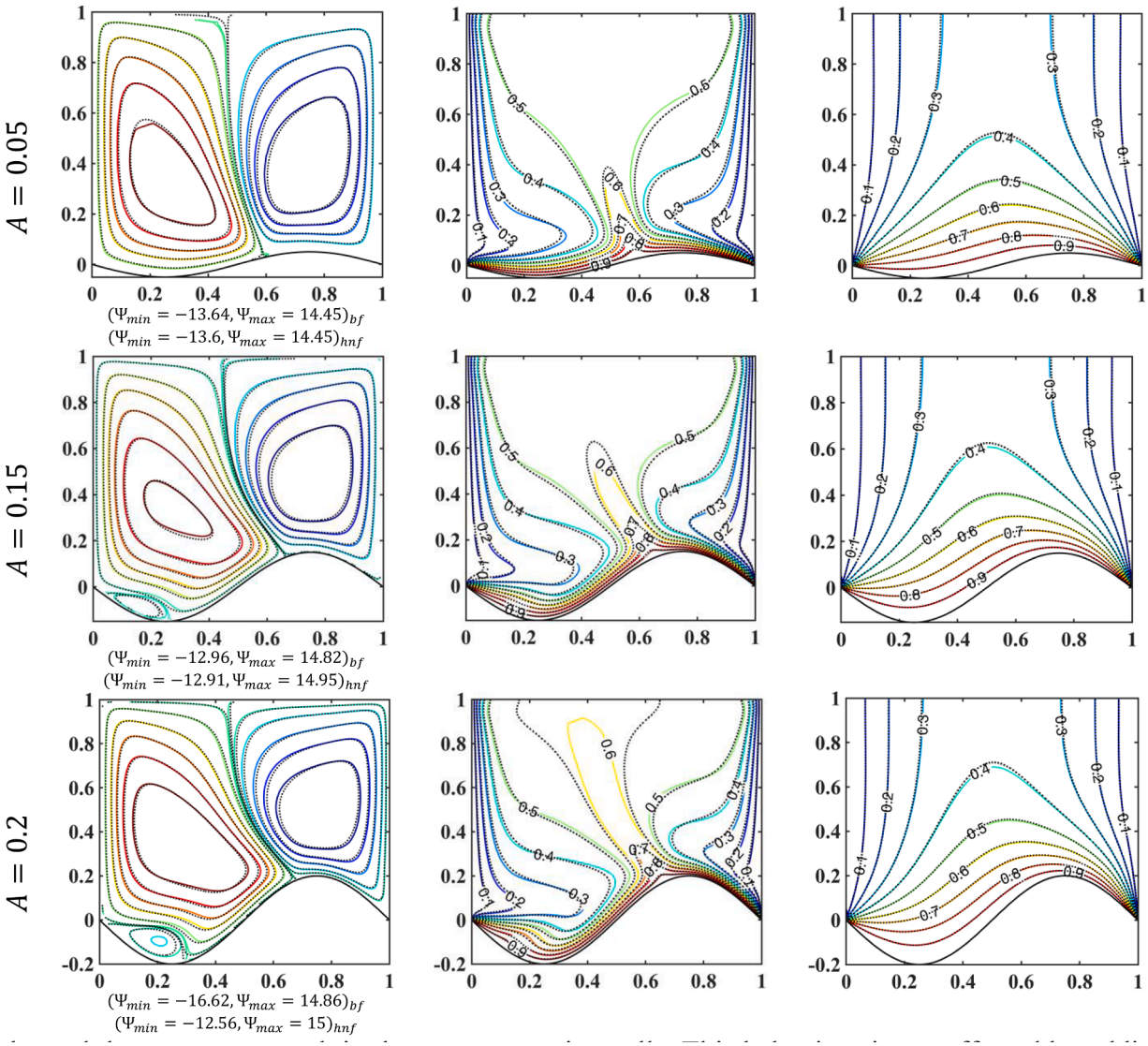

Fig. 5. Variations of (left column) streamlines, (middle column) isotherms of the hybrid nanofluid phase and (right column) isotherms of the solid phase for different amplitude, at γ =10, *N*=2, and $Da = 10^{-3}$, ϕ = 0 (solid lines) and ϕ = 0.04 (dashed lines).

$$where, \varphi = \varphi_{Al_2O_3} + \varphi_{Cu} \tag{14}$$

$$(\rho C_p)_{hnf} = \varphi_{Al_2O_3}(\rho C_p)_{Al_2O_3} + \varphi_{Cu}(\rho C_p)_{Cu} + (\rho C_p)_{bf}(1 - \varphi) \tag{15}$$

The thermal expansion can be defined as:

$$(\rho\beta)_{hnf} = \varphi_{Al_2O_3}(\rho\beta)_{Al_2O_3} + \varphi_{Cu}(\rho\beta)_{Cu} + (\rho\beta)_{bf}(1 - \varphi) \tag{16}$$

where β_{bf}, $\beta_{Al_2O_3}$, and β_{Cu} represent the coefficients of thermal expansion of H_2O, Al_2O_3, and Cu, respectively.

The thermal diffusivity (α_{hnf}) can be defined as:

$$\alpha_{hnf} = \frac{k_{hnf}}{(\rho C_p)_{hnf}} \tag{17}$$

where the thermal conductivity k_{hnf} is defined from the following:

$$\frac{k_{hnf}}{k_{bf}} = \left(\frac{(\varphi_{Al_2O_3}k_{Al_2O_3} + \varphi_{Cu}k_{Cu})}{\varphi} + 2k_{bf} + 2(\varphi_{Al_2O_3}k_{Al_2O_3} + \varphi_{Cu}k_{Cu}) - 2\varphi k_{bf}\right) \times \left(\frac{(\varphi_{Al_2O_3}k_{Al_2O_3} + \varphi_{Cu}k_{Cu})}{\varphi} + 2k_{bf} - 2(\varphi_{Al_2O_3}k_{Al_2O_3} + \varphi_{Cu}k_{Cu}) + 2\varphi k_{bf}\right)^{-1} \tag{18}$$

The effective dynamic viscosity of the hybrid nanofluid is determined as follows:

$$\mu_{hnf} = \frac{\mu_{bf}}{(1 - \varphi)^{2.5}} \tag{19}$$

where μ_{bf} is the dynamic viscosity of pure fluid.

3. Numerical method and validation

To solve the non-dimensional equations with the boundary conditions using the Galerkin finite element method, the Multiphysics COMSOL 5.1 is used. The coupling between the momentum and continuity equations is satisfied using the semi-implicit method for pressure linked equations (SIMPLE). To assess the accuracy of the numerical procedure, a mesh of 120 × 120 is used based on the mesh independent test by the previous work [4].

The set of the dimensionless governing equations with the boundary conditions shown in Section 0 are solved by the Galerkin finite element method as implemented in the Multiphysics COMSOL 5.3 software. The semi-implicit method for pressure linked equations (SIMPLE) algorithm is used to handle the pressure-velocity coupling. The Newton-Raphson method is utilized to simplify the nonlinear terms of the momentum

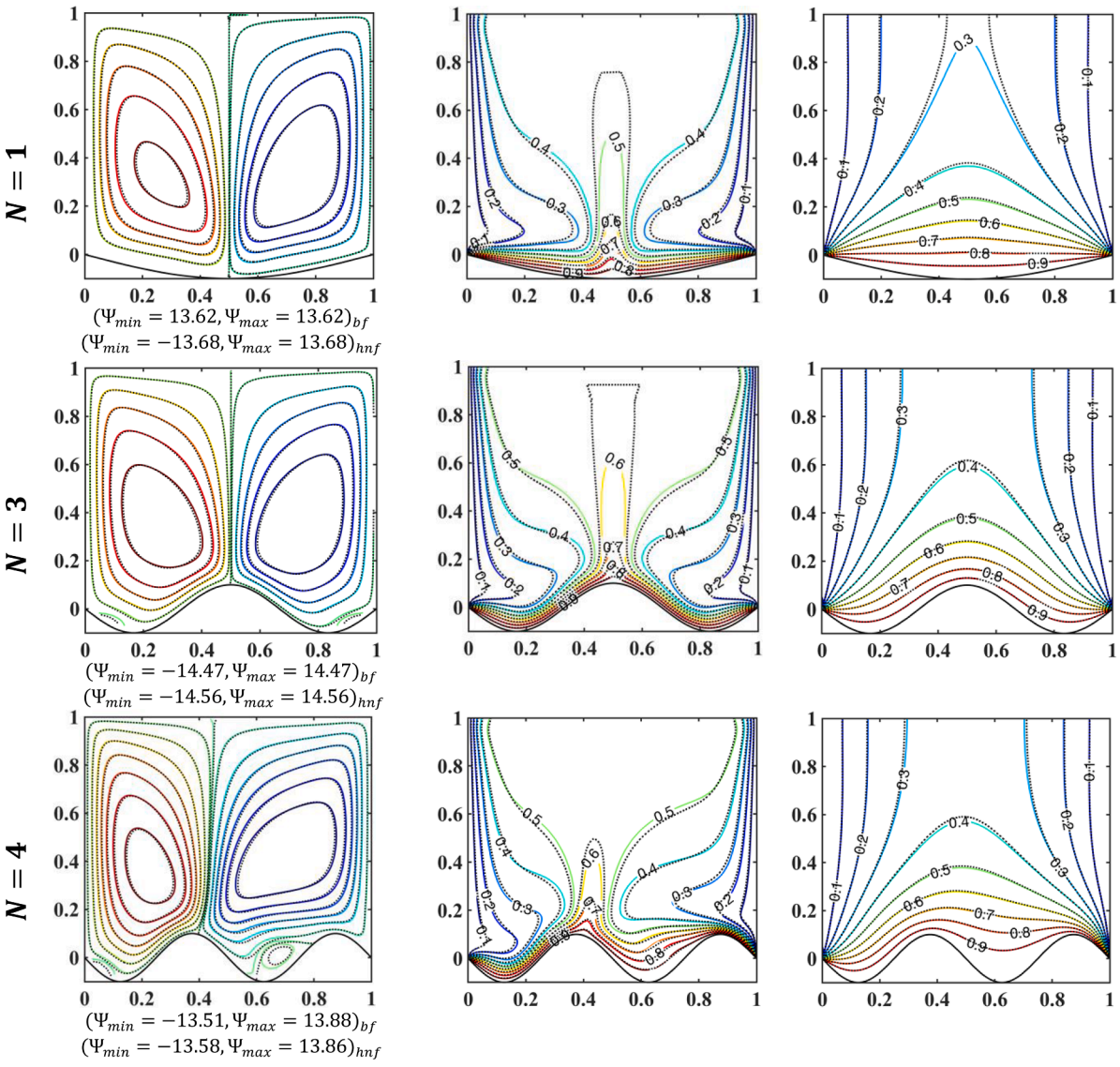

Fig. 6. Variations of (left column) streamlines, (middle column) isotherms of the hybrid nanofluid phase and (right column) isotherms of the solid phase for different wavy wall wavenumbers N at γ =10, A= 1, and $Da = 10^{-3}$, $\phi = 0$ (solid lines) and $\phi = 0.04$ (dashed lines).

equations. This method is considered to have steady solution convergence when the relative error of the specified variables archives the following convergence criteria:

$$\frac{\sum_{i=1}^{I}\sum_{j=1}^{J}\left|\chi_{i,j}^{m+1} - \chi_{i,j}^{m}\right|}{\sum_{i=1}^{I}\sum_{j=1}^{J}\left|\chi_{i,j}^{m+1}\right|} \leq 10^{-6} \tag{25}$$

where i and j represent the ith and jth mesh cell in the directions of the $I \times J$ structured computational domain.

In order to evaluate the dependence of the numerical results on the spatial discretization of the domain, five different size meshes are used to determine the average Nusselt number of the hybrid nanofluid phase (Nu_{hnf}) and the average Nusselt number of the solid phase (Nu_s) for the case of $N = 2$, $A = 0.1$, $H = 10$, $\gamma = 10$, Rayleigh number of $10^6$and Darcy number of 10^{-3}. The above numerical methods are used in the simulations and the boundary conditions are specified in Fig. 1. The predicted results of Table 1 show a very slight difference between mesh of 130 × 130 and above which can be neglected, therefore, the uniform mesh of 130 × 130 is selected for all simulations in the current work.

The current numerical results are validated by comparing them with published numerical results by Baytas [32]. Baytas [32] investigated the impact of local thermal non-equilibrium on the convective flow through a square porous enclosure including heat generation. The case of Fig. 2 from Baytas [32] was studied at $Ra = 10^7$, $Da = 10^{-2}$,$Pr = 7$, $E = 0.4$, $\gamma = 10^{-3}$, F_o= 5.648, and H= 500. The results in Fig. 2 are represent a plot of streamlines and isotherm plots for the fluid and for the porous medium. The predictions from the present study are shown in the lower row of Fig. 2 and the predictions obtained from Baytas [32] are shown in the upper row. A good agreement is observed between the current predicted results and the ones of Baytas [32].

To provide more confidence in the current numerical method, a comparison with the experimental results of Putra et al. [33] and the numerical results of Corcione, et al. [34] are illustrated in Fig. 3. In Fig. 3, the averaged Nusselt number is calculated along the heated wall using Al_2O_3 nanoparticles concentration of 1% at various values of Rayleigh number. The good agreement with the published results gives confidence in the use of the present numerical method.

4. Results and discussion

The results of the numerical simulations are represented by the contours of streamlines and isotherms for the fluid phase and solid

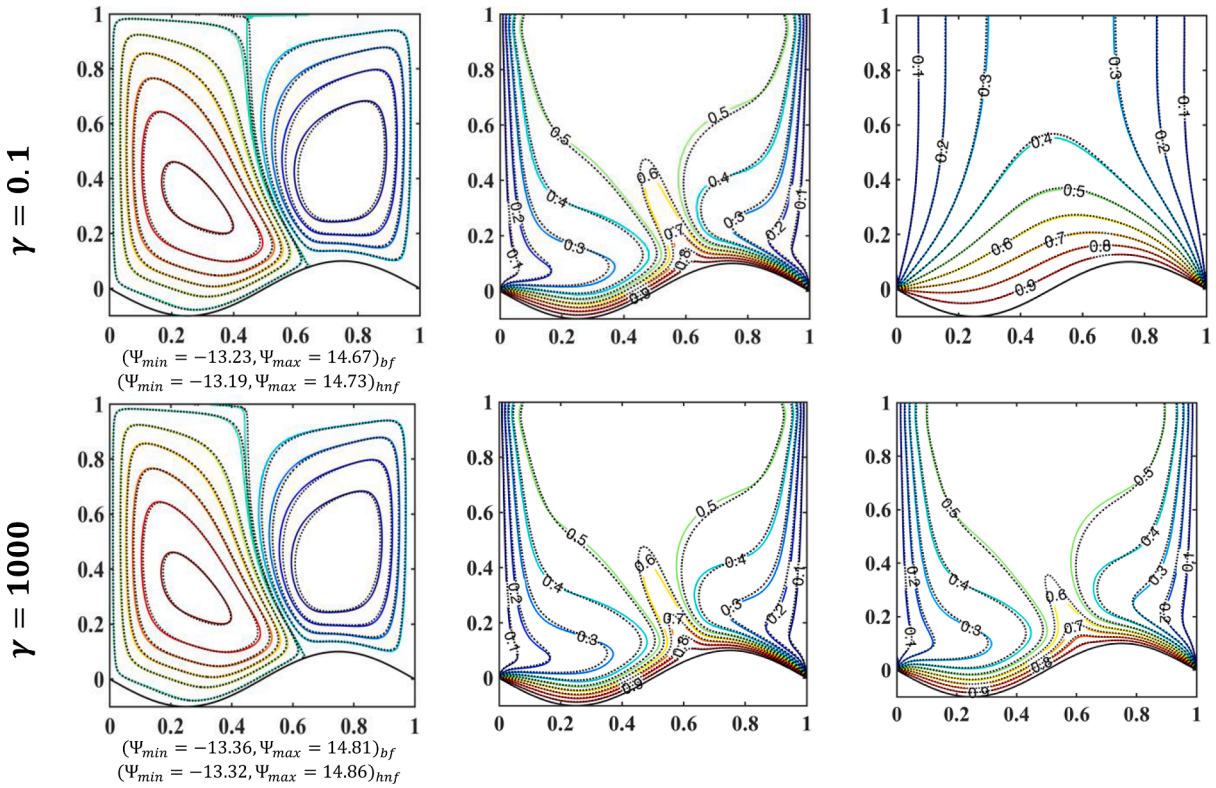

Fig. 7. Variations of (left column) streamlines, (middle column) isotherms of the hybrid nanofluid phase and (right column) isotherms of the solid phase for two values of the modified conductivity ratiosγ, at ϕ = 0(coloured lines) and ϕ = 0.04(black lines).

phase. The average Nusselt number is also plotted along the bottom heated wavy wall at different values of the Darcy number ($10^{-2} \geq Da \geq 10^{-5}$), number of undulations ($1 \leq N \leq 5$), amplitude of waviness ($0.05 \leq A \leq 2$) and the modified conductivity ratio ($0.1 \leq \gamma \leq 1000$). The nanoparticle volume fraction (ϕ) range is $0 \leq \phi \leq 0.04$. The values of Rayleigh number, and the interphase heat transfer coefficient are fixed as $10^6$and 10 respectively.

4.1. Streamlines and isotherms

Fig. 3 shows the impact of the dimensionless Darcy number and of the nanoparticle volume fraction ϕ on temperature distribution for the solid phase (right column), on temperature distribution for the hybrid nanofluid phase (central column), and on streamfunction (left column), at $A = 0.05$, $N = 2$, and $\gamma = 10$. The temperature distributions from the pure water (solid lines) are plotted versus the ones obtained utilizing the hybrid nanofluid (dashed lines). It is showed from the streamlines contour of Fig. 3 that two main recirculation cells are formed inside the enclosure. These vortices are produced due to the buoyancy of the fluid which is heated at the bottom wavy wall and cooled at the right and left vertical walls. The clockwise vortex is located at the left half of the enclosure and the anticlockwise vortex is located at the right half of the enclosure. Qualitatively, as shown in the left column of Fig. 3, the trend of the hybrid nanofluid streamlines is same as the pure fluid as the dashed lines track the solid lines.

Over the selected range of *Da*, the use of 4% by volume of nanoparticles leads to reducing the magnitude of $|\Psi|$ compared to the pure fluid. The reason behind this is the greater dynamic viscosity of the hybrid nanofluid compared to the base fluid which in turn results in a higher viscous dissipation in the hybrid nanofluid. The relative strength of the vortices are varied with the Darcy number. The core of the left recirculation cell is moved towards the to the concave region of the heated wavy wall while the convexity of this wall seems to push the flow. Increasing the Darcy number leads to a significant reduction in the value of the streamlines for both the pure fluid and the hybrid nanofluid.

According to the isotherms in Fig. 3, the isotherms lines tend to be approximately horizontal near the heated wavy wall and they tend to be parallel to the right and left wall vertical walls especially at high value of Darcy number. At the highest value of $Da = 10^{-2}$, the isotherms look denser accumulating near the heated wavy wall following the geometry profile. This density in isotherms shows the increase in temperature gradient which is result from the high conductivity ratio improving convective heat transfer rate. The pattern of isotherms for the pure fluid is consistent with the use of hybrid nanofluid as the dashed lines follow a similar path to the solid lines. The same observation can be seen for the isotherms of the solid matrix in Fig. 3 with a slight change in the temperature gradients over the considered range of Darcy number.

Fig. 4 shows the effect of varying the amplitude of waviness *A* on the convective flow and temperature distributions, at $N = 2$, $Da = 10^{-3}$, and ϕ = 0 and 0.04. At $A = 0.05$, the same pattern of two convection cells of Fig. 3 is observed for the streamlines of Fig. 4 with both pure (solid coloured lines) and Cu-Al_2O_3 hybrid nanofluid (dashed black lines). A small vortex is generated close to the heated wall located at the bottom left corner at $A = 0.15$ and $A = 0.2$. This is because the concave of corrugating walls disturbs the fluid recirculation and the pattern of temperature distributions. For the hybrid nanofluid phase, by increasing the amplitude of the waviness, the isothermal lines of Fig. 5 are distributed inside the entire enclosure with a clear increase in the temperature gradients. This change in temperature distribution can be seen for both the pure fluid and hybrid nanofluid. Whereas, for the solid phase a slight change in the isothermal lines can be observed due to the increment in the amplitude.

The flow and temperature distribution inside the enclosure are significantly affected by the number of undulations *N* at $Da = 10^{-3}$, $A = 0.1$, $\gamma = 10$, as shown in Fig. 5. This can be observed for both pure water, at ϕ = 0 (solid colored lines) and hybrid nanofluid at ϕ = 0.04 (dashed black lines). At $N = 1$, it can be seen that two symmetric convection cells of equal strength are formed inside the enclosure. By increasing *N*, the

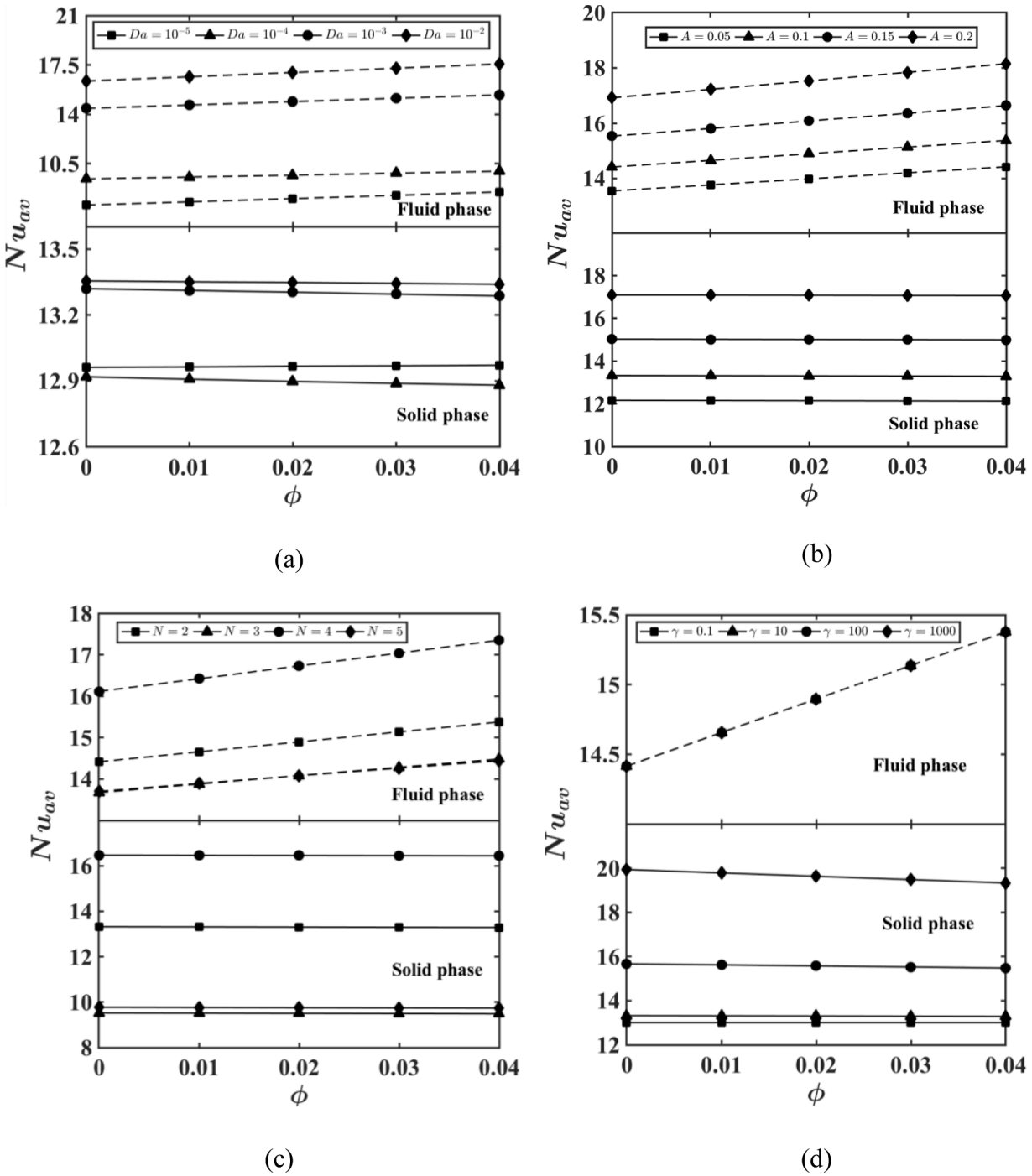

Fig. 8. Variation of the average Nusselt number with ϕ, hybrid nanofluid phase (top) and the solid phase (bottom): (a) *Da* impact, (b) *A* impact, (c) *N*impact, and (d) γ impact.

two circulation cells occupy unequal areas of the enclosure, the clockwise circulation cell on the right is larger. The difference in |Ψ| maxima showed the uneven strength in the two convection cells. This behaviour is not affected by adding 0.04% concentration of nanoparticles as shown by the solid and dashed lines. At $N \geq 3$, secondary recirculation cells adjacent the concave of the heated wavy wall are formed down the main recirculation flow. This is due to the increase in the acceleration of the fluid near the bottom heated wall resulting from the diverging and converging waves. Consequently, the thermal boundary layer thickness is increased as shown in the isotherms of the hybrid nanofluid phase. The isothermal lines are packed to the bottom wavy wall showing a desired wall-normal temperature gradient with good conditions for convective heat transport. The isothermal lines of Fig. 6 follow the undulations of bottom wall for the hybrid nanofluid and solid phases. The right column of Fig. 6 shows the temperature distribution of the solid matrix which indicates the ability of thermal conductivity of the porous matrix to assist the convective heat transfer.

Fig. 7 shows the streamlines and isotherms for the hybrid nanofluid phase and solid phase for different values of the modified conductivity ratio at $\Phi = 0$ (pure fluid) and $\Phi = 0.04$ (hybrid nanofluid). It can observe that two rotating cells are performed in both tested values of the modified conductivity ratio. Increasing γ value has no effect on the vortices pattern for the hybrid nanofluid and pure fluid. A slight change can be observed in the isotherms for the hybrid nanofluid phase. In

contrast, in the solid phase, where a significant difference can be observed in the isotherm's orientation. Besides, the thermal boundary layer thickness is clearly decreased by increasing the modified conductivity ratio. Denser isotherms near the wavy wall which in turn enhances the temperature gradients. At $\gamma = 1000$, the similarity in the isotherms shows that the thermal equilibrium case is achieved.

4.2. Overall heat transfer performance and average Nusselt number

By resolving the Local Thermal Non-Equilibrium (LTNE) in the cavity in Section 4.1, important variations are produced between the temperature distributions in the working fluid and the porous matrix. In this section, the relationship between the average Nusselt number and the nanoparticle volume fraction is explored for different values of Darcy number, amplitude, number of undulations, and modified thermal conductivity ratio. Fig. 7 shows the average Nusselt number on the bottom heated wavy wall of the enclosure for the hybrid nanofluid phase and the solid phase at γ =10, A= 1, and N = 2. Increasing the Darcy number results in a significant increase in the average Nusselt number for the solid and fluid phases among the range of nanoparticle volume fraction. The increase in convection heat transfer is consistent with Fig. 4 (left column) which shows the increase in the strength of the convection cells.

The upper part of Fig. 8b illustrates the Nusselt number based on the fluid temperature differences with the wave amplitude at γ =10, $Da = 10^{-3}$, and N = 2. Increasing the amplitude results in increasing the convection heat transfer rate. This is because the increase in the temperature gradients inside the enclosure as shown in Fig. 4. The bottom part of Fig. 8b illustrates the Nusselt number based on the temperature of the porous matrix with the wave amplitude for different values of nanoparticle concentrations. It is clear from this figure that the volume fraction of nanoparticle concentration has almost no effect on the average Nusselt number. The highest value of amplitude results in the highest value of the average Nusselt number.

Fig. 8c shows the impact of varying the number of undulations on the heat transfer performance for various volume fraction of nanoparticles at γ =10, $Da = 10^{-3}$, and $A = 2$. For the hybrid nanofluid phase, shown in the upper part of Fig. 8, the average Nusselt number is increased by increasing the nanoparticle concentration from 0% to 4%. While for the solid phase, increasing the nanoparticle concentration has almost no impact on the heat transfer performance. Over the range $0 \leq \Phi \leq 0.04$, the highest average number is obtained when the wall wavenumber is N = 4 for both the fluid phase and the solid phase. The average Nusselt number is lowest at $N = 1$ for both the fluid and solid phases. This is also confirmed in the central and right columns of Fig. 6, showing the density of the isothermal lines near the wavy heated wall.

The effect of the modified conductivity ratio on the average Nusselt number at different values of ϕ at $Da = 10^{-3}$, and $A = 2$, $N = 2$ is shown in Fig. 8d For the hybrid nanofluid phase, the heat transfer rate is increased by increasing the nanoparticle volume fraction due to the increase in thermal conductivity with almost no effect from changing γ. In contrast, for the solid phase, a further increase in the modified conductivity ratio resulted in a clear increase in the rate of the heat transfer reaching its maximum value at $\gamma = 1000$.

5. Conclusions

In this study, local thermal non-equilibrium effects are investigated for steady convective heat transfer inside a 2-D porous enclosure having a wavy bottom wall and filled with Al_2O_3Cu/water hybrid nanofluid. By using a Galerkin finite element approach, streamlines, isotherms of the hybrid nanofluid and the solid phases, and the average Nusselt number are evaluated to analyse the flow and heat transfer inside the enclosure over various effective parameters. The key findings of the present study are:

- Darcy number is the most effective variable for controlling the circulation strength of the convective flow and therefore altering rate of the heat transfer.
- Significant impacts of local thermal non-equilibrium are observed at low values of the modified conductivity ratio and high values of Darcy number.
- The increments in the modified conductivity ratio show clear heat transfer enhancement for the solid phase, due to changing the temperature gradients and the thickness of the thermal boundary layer close to the wavy wall.
- Increasing the amplitude A of the bottom corrugated wall results in enhancing the heat transfer performance.
- The number of undulations has uneven effect on fluid flow and heat transfer and the highest heat transfer performance is achieved at N = 4.
- The use of Cu-Al_2O_3 hybrid nanofluid increases the temperature gradients which lead to enhance the rate of heat transfer compared to the pure fluid. At $\phi = 0.04$, $Da = 10^{-3}$ and $N = 4$, the heat transfer performance increases by about 5.45% compared to the pure fluid ϕ = 0 at a constant amplitude $A = 0.1$.

Declaration of Competing Interest

The authors declare that they have no known competing financial interests or personal relationships that could have appeared to influence the work reported in this paper.

Acknowledgements

The authors acknowledge Al-Furat Al-Al-Awsat Technical University for the support to complete the present study. The authors also wish to thank the reviewers for valuable comments and suggestions which have enriched the quality of the paper.

References

[1] A.I. Alsabery, T. Tayebi, A.S. Abosinnee, Z.A.S. Raizah, A.J. Chamkha, I. Hashim, Impacts of amplitude and local thermal non-equilibrium design on natural convection within nanofluid superposed wavy porous layers, Nanomaterials 11 (5) (2021) 1277.
[2] R.S.R. Gorla, S. Siddiqa, M. Mansour, A. Rashad, T. Salah, Heat source/sink effects on a hybrid nanofluid-filled porous cavity, J. Thermophys. Heat Transf. 31 (4) (2017) 847–857.
[3] H.T. Kadhim, F.A. Jabbar, A. Rona, Cu-Al_2O_3 hybrid nanofluid natural convection in an inclined enclosure with wavy walls partially layered by porous medium, Int. J. Mech. Sci. 186 (2020), 105889.
[4] A.J. Chamkha, I.V. Miroshnichenko, M.A. Sheremet, Numerical analysis of unsteady conjugate natural convection of hybrid water-based nanofluid in a semicircular cavity, J. Therm. Sci. Eng. Appl. 9 (4) (2017).
[5] A.I. Alsabery, T. Tayebi, H.T. Kadhim, M. Ghalambaz, I. Hashim, A.J. Chamkha, Impact of two-phase hybrid nanofluid approach on mixed convection inside wavy lid-driven cavity having localized solid block, J. Adv. Res. 30 (2021) 63–74.
[6] S.A. Mehryan, F.M. Kashkooli, M. Ghalambaz, A.J. Chamkha, Free convection of hybrid Al_2O_3-Cu water nanofluid in a differentially heated porous cavity, Adv. Powder Technol. 28 (9) (2017) 2295–2305.
[7] M. Ghalambaz, M.A. Sheremet, S. Mehryan, F.M. Kashkooli, I. Pop, Local thermal non-equilibrium analysis of conjugate free convection within a porous enclosure occupied with Ag–MgO hybrid nanofluid, J. Therm. Anal. Calorim. 135 (2) (2019) 1381–1398.
[8] M. Hirpho, W. Ibrahim, Modeling and simulation of hybrid Casson nanofluid mixed convection in a partly heated trapezoidal enclosure, Int. J. Thermofluids (2022), 100166.
[9] P. Barnoon, Numerical assessment of heat transfer and mixing quality of a hybrid nanofluid in a microchannel equipped with a dual mixer, Int. J. Thermofluids 12 (2021), 100111.
[10] Z. Alhajaj, A. Bayomy, M.Z. Saghir, M.M. Rahman, Flow of nanofluid and hybrid fluid in porous channels: experimental and numerical approach, Int. J. Thermofluids 1 (2020), 100016.
[11] M.M. Ali, R. Akhter, M.A. Alim, Hydromagnetic mixed convection in a triangular shed filled by nanofluid and equipped with rectangular heater and rotating cylinders, Int. J. Thermofluids 11 (2021), 100105.
[12] K.S. Al Kalbani, M. Rahman, M.Z.J.I.J. o. T. Saghir, Entropy generation in hydromagnetic nanofluids flow inside a tilted square enclosure under local thermal nonequilibrium condition, Int. J. Thermofluids 5 (2020), 100031.

[13] Z. Alhajaj, A. Bayomy, M.Z. Saghir, A comparative study on best configuration for heat enhancement using nanofluid, Int. J. Thermofluids 7 (2020), 100041.
[14] A. Kasaeian, et al., Nanofluid flow and heat transfer in porous media: a review of the latest developments, Int. J. Heat Mass Transf. 107 (2017) 778–791.
[15] H. Hashemi, Z. Namazian, S.A.M. Mehryan, Cu-water micropolar nanofluid natural convection within a porous enclosure with heat generation, J. Mol. Liq. 236 (2017) 48–60.
[16] H.T. Kadhim, F.A. Jabbar, A.A. Kadhim, A.K. Jaber, Numerical study of nanofluid flow in a square cavity with porous medium using a sinusoidal interface, in: Proceedings of the 4th Scientific International Conference Najaf (SICN), IEEE, 2019, pp. 216–221.
[17] M. Karim, S. Huq, A. Azad, M. Chowdhury, M.M. Rahman, Numerical analysis of thermofluids inside a porous enclosure with partially heated wall, Int. J. Thermofluids 11 (2021), 100099.
[18] M. Habibishandiz, Z. Saghir, MHD mixed convection heat transfer of nanofluid containing oxytactic microorganisms inside a vertical annular porous cylinder, Int. J. Thermofluids 14 (2022), 100151.
[19] B.M. Al-Srayyih, S. Gao, S.H. Hussain, Effects of linearly heated left wall on natural convection within a superposed cavity filled with composite nanofluid-porous layers, Adv. Powder Technol. 30 (1) (2019) 55–72.
[20] M.T. Nguyen, A.M. Aly, S.W. Lee, Effect of a wavy interface on the natural convection of a nanofluid in a cavity with a partially layered porous medium using the ISPH method, Numer. Heat Transf. Part A Appl. 72 (1) (2017) 68–88.
[21] A. Singh, G. Thorpe, Natural convection in a confined fluid overlying a porous layer-a comparison, Int. J. Heat Mass Transf. 26 (1) (1995) 81–95.
[22] M. Siavashi, R. Yousofvand, S.J.A.P.T. Rezanejad, Nanofluid and porous fins effect on natural convection and entropy generation of flow inside a cavity, Adv. Powder Technol. 29 (1) (2018) 142–156.
[23] I.V. Miroshnichenko, M.A. Sheremet, H.F. Oztop, N. Abu-Hamdeh, M. Transfer, Natural convection of alumina-water nanofluid in an open cavity having multiple porous layers, Int. J. Heat Mass Transf. 125 (2018) 648–657.
[24] A.I. Alsabery, T. Tayebi, A.S. Abosinnee, Z.A. Raizah, A.J. Chamkha, I.J.N. Hashim, Impacts of amplitude and local thermal non-equilibrium design on natural convection within NanoflUid superposed wavy porous layers, Nanomaterials 11 (5) (2021) 1277.
[25] M. Izadi, G. Hoghoughi, R. Mohebbi, M. Sheremet, Nanoparticle migration and natural convection heat transfer of Cu-water nanofluid inside a porous undulant-wall enclosure using LTNE and two-phase model, J. Mole. Liq. 261 (2018) 357–372.
[26] S. Suresh, K. Venkitaraj, P. Selvakumar, M. Chandrasekar, Synthesis of Al_2O_3–Cu/water hybrid nanofluids using two step method and its thermo physical properties, Colloids Surf. A 388 (1–3) (2011) 41–48.
[27] K. Khanafer, K. Vafai, M. Lightstone, Buoyancy-driven heat transfer enhancement in a two-dimensional enclosure utilizing nanofluids, Int. J. Heat Mass Transf. 46 (19) (2003) 3639–3653.
[28] T. Basak, S. Roy, T. Paul, I. Pop, Natural convection in a square cavity filled with a porous medium: effects of various thermal boundary conditions, Int. J. Heat Mass Transf. 49 (7–8) (2006) 1430–1441.
[29] T. Basak, P.K. Pradeep, S. Roy, I. Pop, Finite element based heatline approach to study mixed convection in a porous square cavity with various wall thermal boundary conditions, Int. J. Heat Mass Transf. 54 (9–10) (2011) 1706–1727.
[30] E. Abu-Nada, A.J. Chamkha, Effect of nanofluid variable properties on natural convection in enclosures filled with a CuO–EG–water nanofluid, Int. J. Therm. Sci. 49 (12) (2010) 2339–2352.
[31] H. Brinkman, The viscosity of concentrated suspensions and solutions, J. Chem. Phys. 20 (4) (1952) 571. -571.
[32] A.C. Baytas, Thermal non-equilibrium natural convection in a square enclosure filled with a heat-generating solid phase, non-Darcy porous medium, Int. J. Energy Res. 27 (10) (2003) 975–988.
[33] N. Putra, W. Roetzel, S.K.J.H. Das, M. transfer, Natural convection of Nano-fluids, Heat Mass Transf. 39 (8) (2003) 775–784.
[34] M. Corcione, M. Cianfrini, A. Quintino, Two-phase mixture modeling of natural convection of nanofluids with temperature-dependent properties, Int. J. Therm. Sci. 71 (2013) 182–195.